Journal of Magnetism and Magnetic Materials 427 (2017) 143–149

Contents lists available at ScienceDirect

Journal of Magnetism and Magnetic Materials

journal homepage: www.elsevier.com/locate/jmmm

Three-dimensional magnetic nanoparticle imaging using small field gradient and multiple pickup coils

Teruyoshi Sasayama*, Yuya Tsujita, Manabu Morishita, Masahiro Muta, Takashi Yoshida, Keiji Enpuku

Department of Electrical Engineering, Kyushu University, Fukuoka 819-0395, Japan

ARTICLE INFO

Keywords:
Magnetic particle imaging
Multiple pickup coils
Gradient field
Nonnegative least squares method
Three-dimensional imaging

ABSTRACT

We propose a magnetic particle imaging (MPI) method based on third harmonic signal detection using a small field gradient and multiple pickup coils. First, we developed a system using two pickup coils and performed three-dimensional detection of two magnetic nanoparticle (MNP) samples, which were spaced 15 mm apart. In the experiments, an excitation field strength of 1.6 mT was used at an operating frequency of 3 kHz. A DC gradient field with a typical value of 0.2 T/m was also used to produce the so-called field-free line. A third harmonic signal generated by the MNP samples was detected using the two pickup coils, and the samples were then mechanically scanned to obtain field maps. The field maps were subsequently analyzed using the nonnegative least squares method to obtain three-dimensional position information for the MNP samples. The results show that the positions of the two MNP samples were estimated with good accuracy, despite the small field gradient used. Further improvement in MPI performance will be achieved by increasing the number of pickup coils used.

1. Introduction

Magnetic nanoparticles (MNPs) have been widely studied for use in biomedical applications. One of these applications is the so-called magnetic particle imaging (MPI), which is used to detect the positions and numbers of MNPs that are accumulated in a human (or animal) body for in vivo medical diagnosis purposes [1–12]. In this application, the MNPs are magnetized using an excitation field, and the resulting signal from the MNPs is detected using one or multiple pickup coil(s). The positions and numbers of the MNPs can then be reconstructed from the measured data through solution of an inverse problem.

The signal that is detected using the pickup coil, B_s, is known to be determined by two terms. The first term is the response of the MNPs to the excitation field, i.e., the magnetization signal B_{MNP}. The other term is the relative distance between the MNPs and the pickup coil. Based on these characteristics, three typical MPI methods have been developed.

The first method involves application of a homogeneous AC excitation field and measurement of the contour map of the signal field generated by the MNP sample [1–3]. In this case, the relative distance between the MNPs and the pickup coil varies at each measurement point. This means that the contour map includes the required information about the spatial distribution of the MNPs. The MNP distribution can therefore be reconstructed from the contour map by solving the inverse problem. While this method requires a relatively simple measurement system, the spatial resolution of MNP detection is reduced when the MNPs are located far away from the pickup coil. This is because the signal field broadening increases in this case.

The second method involves use of an inhomogeneous AC excitation field [4,5]. In this case, the excitation field strength is spatially distributed, and B_{MNP} for the MNPs is determined by the excitation field at the MNP positions. Therefore, if the distribution of the excitation field is known beforehand, additional information about the spatial distribution of the MNPs can be obtained based on B_{MNP}. As a result, the contour map of the signal field obtained using the inhomogeneous excitation field contains much more information about the MNP spatial distribution than that in the homogeneous excitation field case. While the spatial resolution of MNP detection can be improved using this method, this spatial resolution is significantly dependent on the excitation field distribution profile. Therefore, optimum inhomogeneous excitation field design is a crucial factor.

The third method involves the use of an additional DC gradient field to produce the so-called field-free point (FFP) [6–12]. Because of the properties of the MNPs, the magnetization signal B_{MNP}, which is composed of harmonic signals, is generated selectively from the MNPs that are located at the FFP. This means that the information with regard to the MNP spatial distribution can be acquired using the

* Corresponding author.
E-mail address: sasayama@sc.kyushu-u.ac.jp (T. Sasayama).

http://dx.doi.org/10.1016/j.jmmm.2016.10.107
Received 22 June 2016; Received in revised form 17 October 2016; Accepted 19 October 2016
Available online 23 October 2016
0304-8853/

FFP. The signal field from the MNPs located at the FFP can be detected using a large pickup coil. By three-dimensional scanning of the FFP, we can obtain the spatial distribution of the MNPs. While high spatial resolution can be achieved in MNP detection, we need to develop a gradient coil that can generate a strong field gradient (typically 1–2 T/m). This is because MPI spatial resolution is proportional to the field gradient. Additionally, we also need to develop a method to perform three-dimensional scanning of the FFP.

In our previous work, we developed a two-dimensional MPI system that used third-harmonic signal detection and the FFP [12]. In this system, we used a relatively low AC excitation field (1.6 mT) and small field gradient (0.3 T/m). We demonstrated spatial resolution of 10 mm with this system, despite the low field gradient. This was achieved using the properties of the MNPs. Specifically, the field gradient, which is necessary to maintain the spatial resolution of the process, can be reduced by reducing the excitation field, as shown in Ref. [13]. As a result, we were able to use a compact power supply for the coil systems.

In this work, we extend the previous system to develop three-dimensional MPI. For this system, we use a gradient field that produces a field-free line (FFL). We also use multiple pickup coils for signal detection. This combination of the FFL with multiple pickup coils allows us to obtain three-dimensional information about the spatial distribution of the MNPs. We first developed an MPI system that used two pickup coils and a field gradient of approximately 0.2 T/m. Using the resulting system, we then performed three-dimensional detection of two MNP samples. The signal field contour maps were measured using the two pickup coils when the MNP samples were mechanically scanned. Then, we reconstructed the three-dimensional distribution of the MNPs from the measurement contour maps by solving the inverse problem using the nonnegative least squares (NNLS) method.

2. Method

2.1. Measurement system

Fig. 1 shows a schematic depiction of the MPI system using third-harmonic signal detection. The system was previously described in detail in Refs. [12] and [14]. The measurement system consists of three coils, which are the excitation, pickup, and gradient coils. The excitation coils are 300 mm in diameter and are spaced 300 mm apart. An excitation field B_{ac} with a root mean square value of 1.6 mT and an operating frequency of f =2.93 kHz was applied along the y direction via the excitation coils. An MNP sample was magnetized by the excitation field and generated a third harmonic signal B_s at f =8.79 kHz as a result because of the nonlinear magnetization of the MNP sample. The z-component of the signal field was then detected using the two pickup coils.

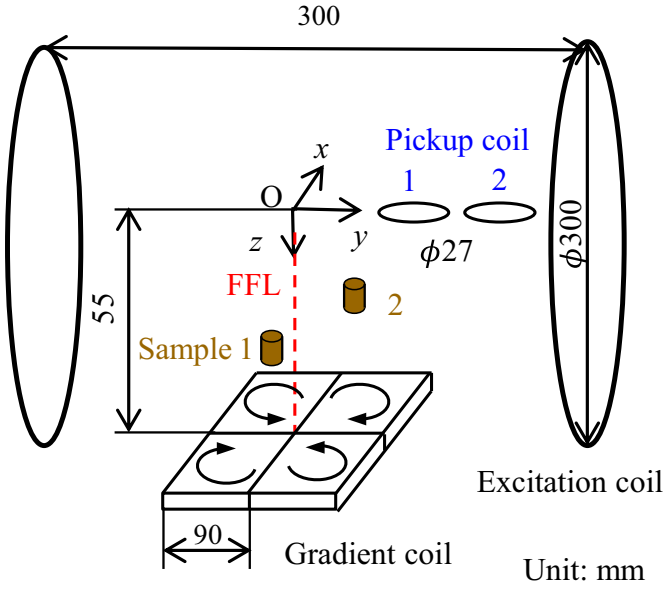

Fig. 1. Schematic diagram of measurement system.

Pickup coils 1 and 2 were set at positions (x_p, y_p, z_p) =(0, 15 mm, 0) and (0, 60 mm, 0) in xyz coordinates, respectively, as shown in Fig. 1. The pickup coils were made from Cu Litz wire, and the average diameter and number of turns of these coils were D =27 mm and N =200, respectively. The coils were cooled to 77 K using liquid nitrogen to reduce thermal noise. The inductances of pickup coils 1 and 2 were L_1 =0.927 mH and L_2 =0.937 mH, respectively, and the corresponding resistances were R_1 =0.43 Ω and R_2 =0.41 Ω at T=77 K, respectively. Pickup coils 1 and 2 were connected to resonant capacitances of C_1 =0.3581 μF and C_2 =0.3351 μF, respectively, to enhance the third harmonic signal that is generated in the pickup coils. The resulting voltage was amplified using a low-noise preamplifier (SA-421F5, NF Corp.), and the third harmonic signal was then measured using a lock-in amplifier (LI5640, NF Corp.). The magnetic field noise of the detection system reached a minimum at the resonant frequency. We obtained the magnetic field noise of the pickup coil $S_B^{1/2}$ =9 fT/Hz$^{1/2}$ at a signal frequency of f =8.79 kHz.

The gradient field was generated using a planar coil that consisted of four square coils, as shown in Fig. 1 [12]. Each of these square coils had an average side length of 90 mm and comprised 200 turns. A DC current of 3.5 A was supplied to the gradient coil in the direction shown in Fig. 1.

Fig. 2 shows the calculated distribution of the magnetic field generated by the gradient coil. Fig. 2(a) shows the distribution of $|\boldsymbol{B}_{dc}|$ in the yz plane at x=0, where $|\boldsymbol{B}_{dc}|$ is the absolute value of the DC gradient field. As shown, $|\boldsymbol{B}_{dc}|$ becomes zero along the z axis, i.e., along the line that passes through the center of the gradient coil. The FFL was therefore generated along this line.

Fig. 2(b) shows the distribution of $|\boldsymbol{B}_{dc}|$ in the xy plane at z=50 mm. It can be shown that the gradient field mainly has x and y components near the FFL, and the field distribution can then be expressed approximately as

$$\boldsymbol{B}_{dc}=(Gy,\ Gx,0), \tag{1}$$

where G is the field gradient. The value of G varied from 0.15 to 0.25 T/m as the z position changed from 30 to 50 mm.

As shown in Fig. 1, the combination of the FFL and the two pickup coils was used in the method presented here to obtain the required information about the three-dimensional positioning of the MNP sample. When the sample is scanned in the xy plane around the FFL, a high third-harmonic signal is generated by the sample. Therefore, the MNP distribution in the xy plane can be acquired using the FFL. We note that the FFL is essential for improved spatial resolution, although the field gradient is small. The spatial resolution deteriorates dramatically if we do not use the FFL.

However, we cannot obtain sufficient information about the MNP distribution along the z axis using a single pickup coil. Two pickup coils were therefore used to increase the information that is acquired. Because pickup coils 1 and 2 have different distances r for the same sample, we can obtain the required information on r from a comparison of the signal fields measured using pickup coils 1 and 2. In particular, the information required about the z-position of the sample can be obtained. In this manner, we can acquire the three-dimensional position information for the MNP sample using the combination of the FFL with multiple pickup coils.

2.2. Imaging procedure

In this experiment, three-dimensional detection of two MNP samples was performed using the following procedure. First, the two MNP samples were set at different sample positions, denoted by (x_s, y_s,

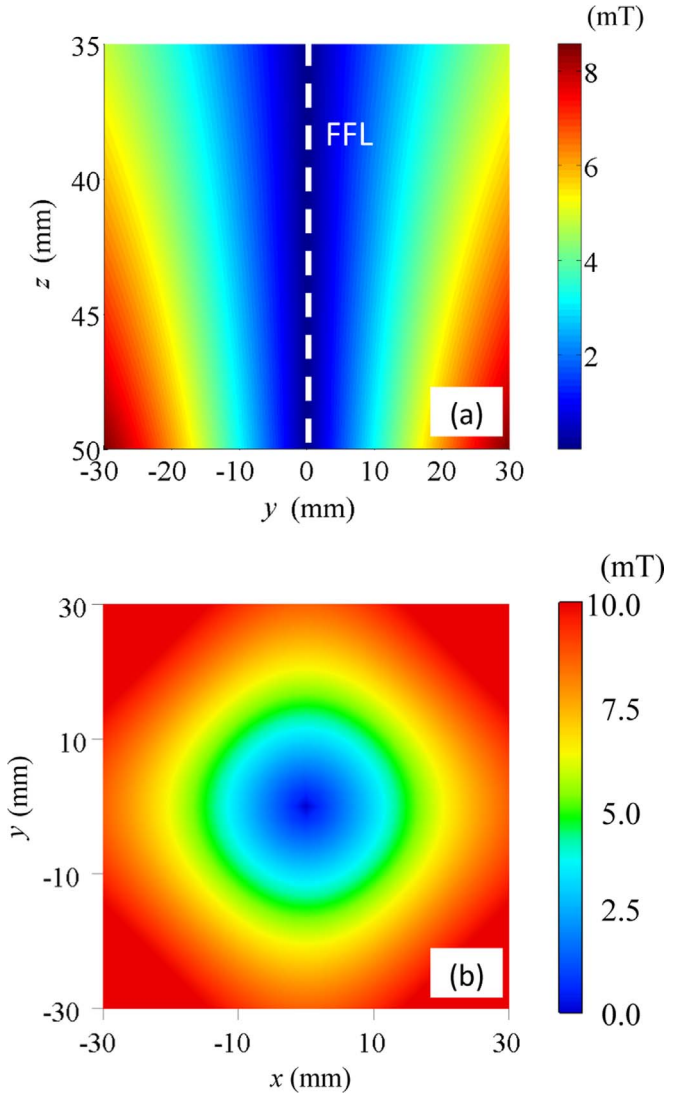

Fig. 2. Distribution of $|\boldsymbol{B}_{dc}|$ in (a) the yz plane at x=0, and (b) the xy plane at z=50 mm. The field was calculated when a 3.5 A DC current was supplied to the gradient coil.

z_s) in xyz coordinates, as shown in Fig. 1. The two MNP samples were set on a single sample holder.

The sample holder was then mechanically scanned in the xy plane at a speed of 20 mm/s while the coil systems remained fixed. Note here that the samples were only scanned in two dimensions, rather than in three dimensions. By scanning the sample holder, we then obtained a field map from the MNP samples using pickup coils 1 and 2. The field map is represented by a signal vector $\boldsymbol{v}_k$ (where k=1, 2). The scanned area had dimensions of 80 mm×80 mm, and the field map resolution was set at 2 mm×2 mm. We thus obtained a signal vector $\boldsymbol{v}_k$ with 41×41=1681 components from the pickup coil k (where k=1, 2).

Finally, we analyzed the measured field map using the signal vector $\boldsymbol{v}_k$ to reconstruct a three-dimensional distribution of the MNP concentration. Here, we assume that the MNPs exist in the volume Ω with dimensions of 60 mm×60 mm×30 mm, i.e., in the ranges where −30 mm ≤ x≤30 mm, −30 mm ≤ y≤30 mm, and 25 mm ≤ z≤55 mm in xyz coordinates, as shown in Fig. 1. Suppose that the MNPs are distributed with a concentration $c(\boldsymbol{r})$, (where $\boldsymbol{r}\in\Omega$). The signal vector $\boldsymbol{v}_k$ that was obtained from pickup coil k can then be expressed as

$$\boldsymbol{v}_k=\boldsymbol{A}_k\boldsymbol{c}, \tag{2}$$

where $\boldsymbol{A}_k$ is the system function matrix [7,15] for pickup coil k, and $\boldsymbol{c}$ denotes a vector with components that are determined by $c(\boldsymbol{r})$. The model given by Eq. (2), which assumes that multiple signal sources are distributed at the lattice points, is also used in signal source estimation processes in electroencephalography and magnetoencephalography applications [16].

The concentration $\boldsymbol{c}$ was then determined by solving Eq. (2) using the NNLS method as follows:

$$\boldsymbol{c}=\underset{\boldsymbol{c}}{\operatorname{argmin}}\left\|\begin{pmatrix}\boldsymbol{A}_1\\ \boldsymbol{A}_2\end{pmatrix}\boldsymbol{c}-\begin{pmatrix}\boldsymbol{v}_1\\ \boldsymbol{v}_2\end{pmatrix}\right\|^2+\lambda\|\boldsymbol{c}\|^2\ (\boldsymbol{c}\geq 0), \tag{3}$$

where λ is a regularization parameter. The NNLS problem shown in Eq. (3) was solved using Optimization Toolbox from MATLAB 2015a (Mathworks Inc).

To solve Eq. (3), we set the element pixel size for estimation of the $\boldsymbol{c}$ distribution to 2 mm×2 mm×5 mm in xyz coordinates. In this case, $\boldsymbol{c}$ has 31×31×7=6727 components. The value of $\boldsymbol{A}_k$ becomes equal to that of $\boldsymbol{v}_k$ when a point (i.e., infinitely small) sample is scanned in the volume Ω, and this is called a point spread function. This point spread function can be obtained both analytically and experimentally [15].

3. Experiment

3.1. Measured field map

In our experiments, we used commercial magnetic nanoparticles called Resovist (Fujifilm RI Pharma). The Resovist sample was magnetically fractionated so that the particles have large magnetic moments [17]. The original MNP solution was diluted using glycerol to obtain a 150 μl sample with 10 μg of Fe content. The sample was enclosed in a cylindrical cell that was approximately 6 mm in diameter with a height of 5 mm.

Fig. 3 shows the field map that was measured when the two MNP samples were set at (x_s, y_s, z_s) =(−7.5 mm, −7.5 mm, 35 mm) and (7.5 mm, 7.5 mm, 50 mm). The z-position of the MNP sample, denoted by z_s, was chosen with breast cancer detection applications in mind [1]. Fig. 3(a) and (b) show the field maps that were measured using pickup coils 1 and 2, respectively. The open circles in the figure indicate the positions and sizes of the MNP samples when projected on the xy plane. As shown in the figures, the measured fields were high at these positions. Note that different field maps were obtained by the two coils, as shown by comparison of Fig. 3(a) and (b).

Fig. 4 shows the field maps that were measured when the two MNP samples were set at (x_s, y_s, z_s) =(0, 0, 35 mm) and (0, 0, 50 mm). In this case, only the z positions of the MNP samples differed. Figs. 4(a) and (b) show the field maps that were measured using pickup coils 1 and 2, respectively. The difference between the two maps is smaller in this case than that shown in Fig. 3. As a result, it was difficult to distinguish between the two MNP samples when using the field maps.

3.2. System function A_k

To reconstruct the MNP concentration ($\boldsymbol{c}$) from the measured field map ($\boldsymbol{v}_k$) given by Eq. (3), we need to know the system function $\boldsymbol{A}_k$. In this study, the value of $\boldsymbol{A}_k$ was obtained experimentally by measuring the point spread function. The step size for reconstruction in the z direction was set at 5 mm, and we thus obtained $\boldsymbol{A}_k$ at intervals of 5 mm in the z direction; i.e., the values of $\boldsymbol{A}_k$ were obtained when the point sample was scanned on the xy plane at z=25, 30, 35, 40, 45, 50, and 55 mm.

Fig. 5 shows the system function of pickup coil 1, i.e., $\boldsymbol{A}_1$, which was obtained in this manner. Figs. 5(a) and (b) represent the values of $\boldsymbol{A}_1$ at z=25 mm and 55 mm, respectively. Fig. 5(c) shows the distribution of $\boldsymbol{A}_1$ in the x direction at y=0. The figure shows that the full width at half maximum (FWHM) at z=55 mm is smaller than that at z=25 mm. This is because the gradient field intensity increased with increasing z in this experimental setup.

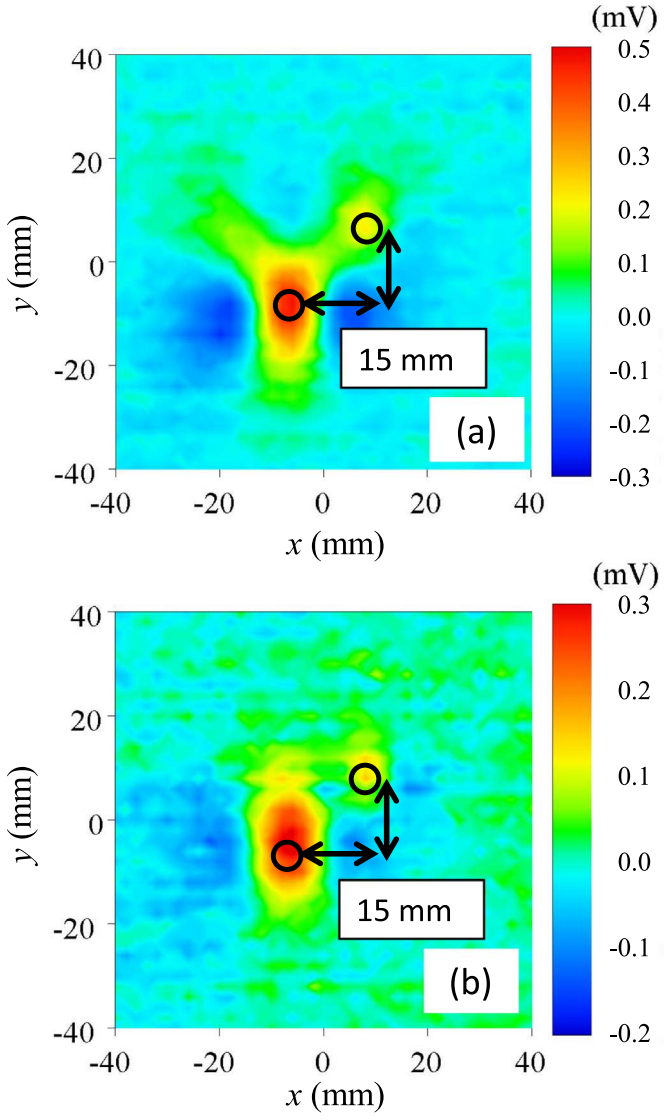

Fig. 3. Field maps for two MNP samples located at (x_s, y_s, z_s) =(−7.5 mm, −7.5 mm, 35 mm) and (7.5 mm, 7.5 mm, 50 mm). (a) and (b) show field maps that were measured using pickup coils 1 and 2, respectively. Open circles indicate the positions and sizes of the two MNP samples when projected on the *xy* plane.

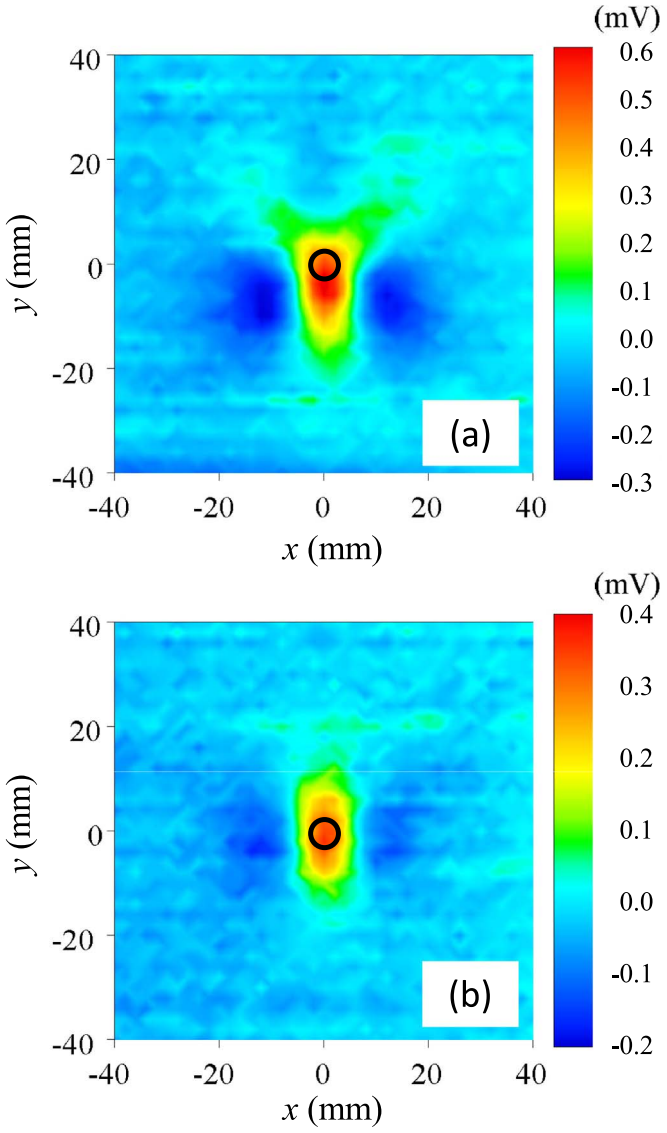

Fig. 4. Field maps for two MNP samples located at (x_s, y_s, z_s) =(0, 0, 35 mm) and (0, 0, 50 mm), as measured using (a) pickup coil 1 and (b) pickup coil 2.

3.3. Three-dimensional imaging results

Fig. 6 shows the three-dimensional imaging results for the MNP samples. The three-dimensional concentration $\boldsymbol{c}$ of the MNPs was reconstructed based on the field maps that were shown in Fig. 3 using Eq. (3).

The time that was required to obtain the $\boldsymbol{c}$ distribution was as follows. The imaging time for the signal field contour maps was approximately 12 min. The system function acquisition time was approximately 130 min. The reconstruction time required to solve Eq. (3) was approximately 1–2 min.

To solve Eq. (3), the value of the regularization parameter λ was set at $\lambda=5.0\times10^{-6}$; note that almost identical results were obtained for values ranging between $\lambda=1.0\times10^{-6}$ and 1.0×10^{-7}. Because the system function $\boldsymbol{A}_k$ was obtained at intervals of 5 mm in the *z* direction, the concentration $\boldsymbol{c}$ was also obtained at 5 mm intervals in the *z* direction. Therefore, in Fig. 6(a), the distribution of $\boldsymbol{c}$ in the *xy* plane is shown at 5 mm intervals in the *z* direction.

As Fig. 6(a) shows, two maxima were obtained in the MNP concentration. These maxima correspond to the two MNP samples, and their positions are shown to be clearly separated. These results indicate that the MNP samples were clearly detected in a three-dimensional manner.

Table 1 lists the positions of the two MNP samples that were estimated from the results in Fig. 6(a). The two positions were estimated to be (*x*, *y*, *z*) =(−8 mm, −6 mm, 35 mm) and (8 mm, 8 mm, 50 mm). As shown in Table 1, the estimated positions agree well with the actual sample positions, with a position estimation error of approximately 1 mm in the *xy* plane. Accurate three-dimensional estimation of the positions of MNPs is therefore possible, despite the low field gradient of approximately 0.2 T/m that was used in the experiments.

Fig. 6(a), however, also shows that artifacts existed in the estimated MNP concentration. These artifacts mainly appeared at more distant positions, i.e., at higher values of *z*. This is because the signal-to-noise ratio (SNR) of the signal field was smaller for the MNPs that were located in these distant positions. It is thus necessary to improve the SNR to reduce the occurrence of these artifacts.

Fig. 6(b) shows the MNP concentration when projected on the *xy* plane. The open circles represent the positions and the sizes of the two MNP samples that were projected on the *xy* plane. As shown, the size of the MNP image was smaller than that of the actual sample. The color bar shown in Fig. 6 represents the value of $\boldsymbol{c}$ in units of μg-Fe/pixel. By

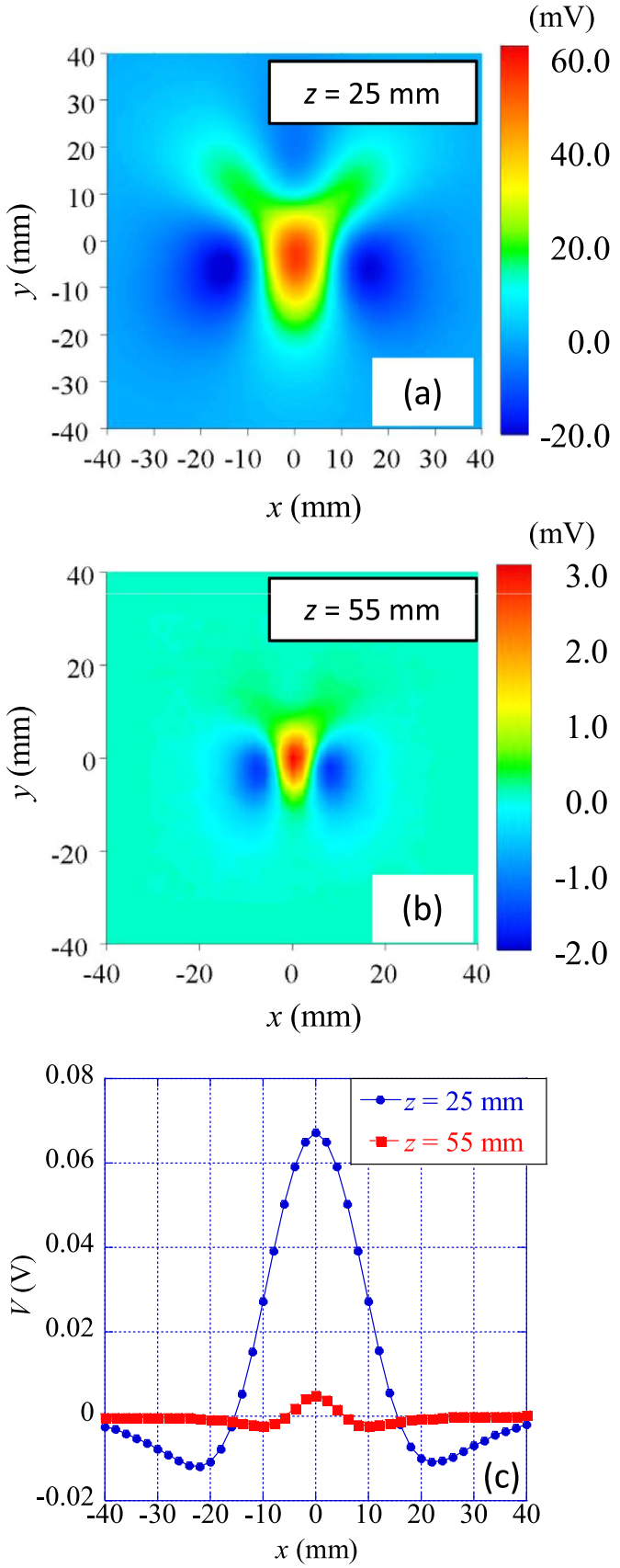

Fig. 5. System function A_1 of pickup coil 1 for (a) z=25 mm and (b) z=55 mm. (c) Distribution of A_1 in x direction at y=0.

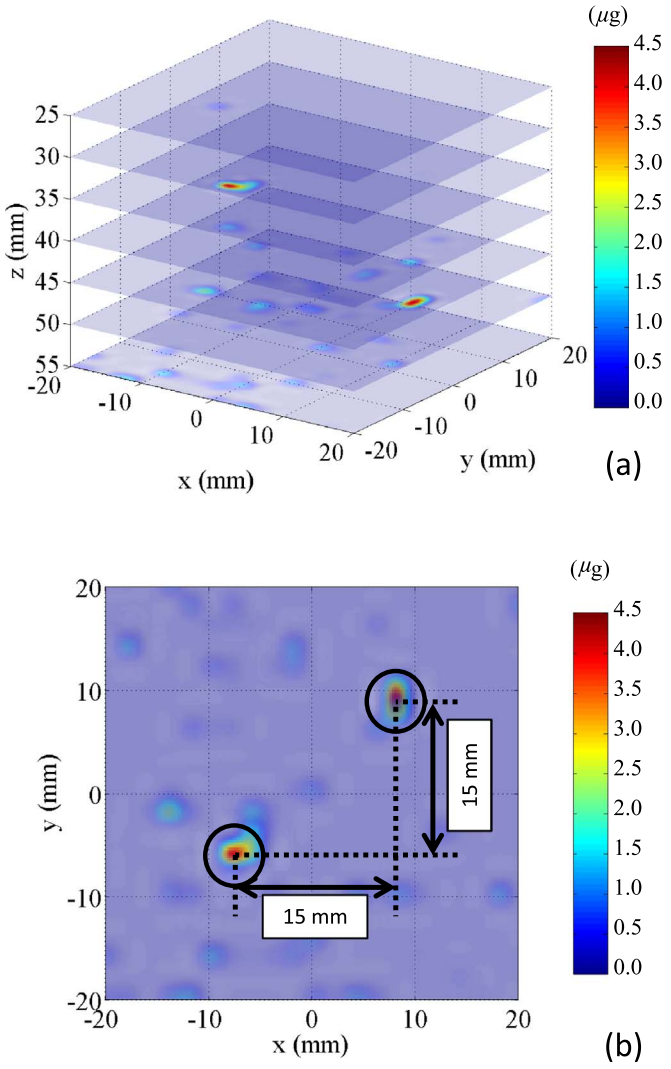

Fig. 6. Distribution of the MNP concentration that was obtained from the field maps shown in Fig. 3, where the two MNP samples were located at (x_s, y_s, z_s) =(−7.5 mm, −7.5 mm, 35 mm) and (7.5 mm, 7.5 mm, 50 mm). (a) Three-dimensional imaging of the MNP concentration, and (b) concentration of MNPs when projected on the xy plane. Open circles represent the positions and sizes of the two MNP samples when projected on the xy plane. The color bar represents the value of $\boldsymbol{c}$ in units of μg-Fe/pixel.

Table 1
Actual and estimated position results for the case shown in Fig. 6.

	Actual position			Estimated position		
	x (mm)	y (mm)	z (mm)	x (mm)	y (mm)	z (mm)
Sample 1	−7.5	−7.5	35	−8	−6	35
Sample 2	7.5	7.5	50	8	8	50

integrating the concentration $\boldsymbol{c}$ around the MNP sample, we estimated the quantities of Fe to be 8.2 and 7.7 μg for the two MNP samples. These estimated values were lower than the actual Fe quantity of 10 μg.

We believe that the errors noted above in the size and quantity of the reconstructed $\boldsymbol{c}$ occurred because only two pickup coils were used in the experiment. We have performed numerical simulations of the system when higher numbers of pickup coils are used. These simulations indicate that the accuracy of reconstruction of the quantity and size of the sample can be enhanced by increasing the number of pickup coils used from two to five. An MPI system using five pickup coils will therefore be useful for further performance improvements.

Fig. 7 shows the three-dimensional imaging results that were

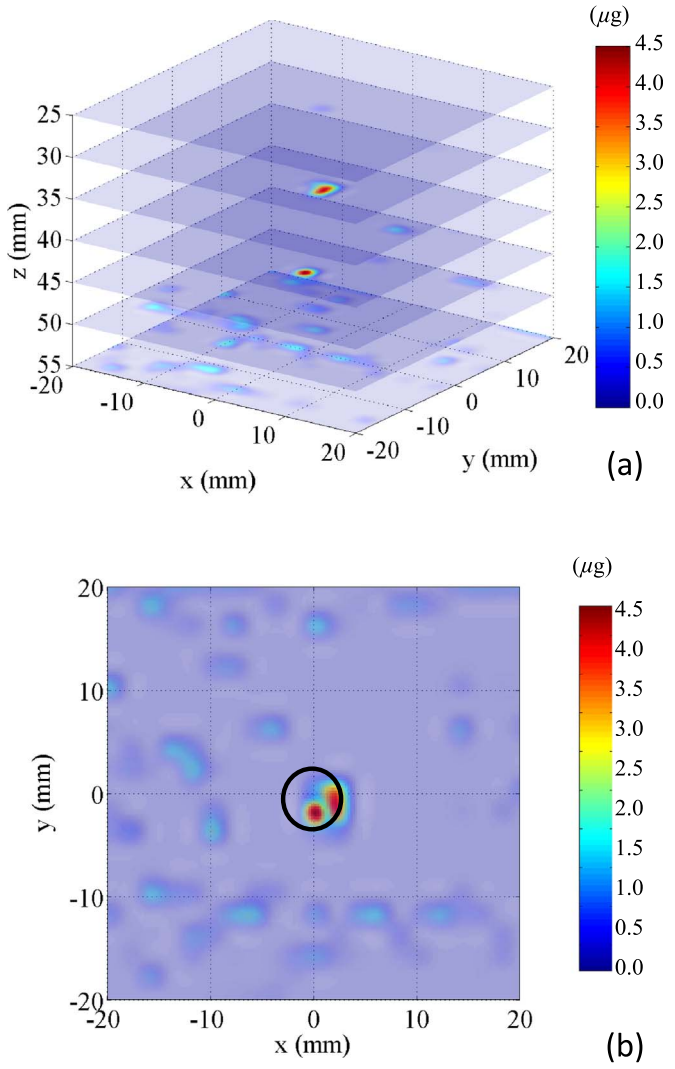

Fig. 7. Distribution of MNP concentration obtained from field maps shown in Fig. 4, in which the two MNP samples were located at (0, 0, 35 mm) and (0, 0, 50 mm). (a) Three-dimensional imaging of the MNP concentration, and (b) MNP concentrations projected on the *xy* plane.

Table 2
Actual and estimated position results for the case shown in Fig. 7.

	Actual position			Estimated position		
	x (mm)	*y* (mm)	*z* (mm)	*x* (mm)	*y* (mm)	*z* (mm)
Sample 1	0	0	35	2	0	35
Sample 2	0	0	50	0	−2	50

obtained based on the field maps shown in Fig. 4. In this case, the two MNP samples were located at (x_s, y_s, z_s) =(0, 0, 35 mm) and (0, 0, 50 mm), i.e., only the *z* positions of the two MNP samples were different. This limited difference made it difficult to distinguish between the two MNP samples when using the field maps, as shown in Fig. 4.

Fig. 7(a) shows the three-dimensional MNP concentration distribution. The figure shows that the two MNP samples can be clearly distinguished even in this case. This result illustrates the usefulness of the method presented here for improved spatial resolution in MNP detection.

Table 2 shows the position estimation results for the case shown in Fig. 7. The estimated position results for the two MNP samples again agree well with the actual sample positions.

Fig. 7(b) shows the MNP concentration when projected on the *xy* plane. As the figure shows, the MNP image size was smaller than the actual sample size. The quantities of Fe were estimated to be 8.8 and 6.7 μg for the two MNP samples, which were both lower than the actual Fe quantity of 10 μg. These results are similar to those given in Fig. 6(b).

Finally, we note that it will be necessary to detect several MNP samples with different concentrations in practical applications. For this purpose, it will thus also be necessary to estimate the positions, sizes and quantities of the MNP samples more accurately. As discussed with reference to Fig. 6, it will be useful to increase the number of pickup coils used for this purpose, e.g., the use of five pickup coils proposed here. This is because we can solve Eq. (3) with greater accuracy by increasing the number of vectors v_k, as long as all v_k are linearly independent.

We also note that it is important that the field maps are obtained with suitably high SNRs. When the SNR was low, artifacts began to appear in the estimated MNP concentrations, as shown in Figs. 6 and 7. We must also select a suitably large regularization parameter λ in Eq. (3), when the SNR is low. In the case of large λ value, however, the spatial resolution of the estimated MNP distribution becomes degraded.

4. Conclusions

In this study, we developed an MPI system based on third-harmonic signal detection. By using the properties of the MNPs, we were able to use a low field gradient (0.2 T/m) without degrading the spatial resolution through use of a small excitation field (1.6 mT). Because we can use compact power supplies for the coil systems, upscalling of the method presented here will be comparatively simple. The combination of the FFL and two pickup coils was used to acquire the three-dimensional position information of the MNP samples. The field maps were measured using the two pickup coils by scanning the sample in a two-dimensional manner. Then, the inversion problem for MPI was solved using the NNLS method. In the method presented, two-dimensional scanning of the sample is sufficient for reconstruction of three-dimensional MNP images. We also successfully demonstrated three-dimensional detection of two MNP samples. These results confirmed the usefulness of the method presented in this work. Further improvements in MPI performance will be achieved through the use of five pickup coils. We note, however, that the temporal resolution of the MPI is not high because the presented method used a resonant circuit to perform the measurements. Therefore, this method is useful when high temporal resolution is not required.

Acknowledgements

This work was partly supported by a Grant-in-Aid for Scientific Research (S) from the Japan Society for the Promotion of Science [grant number 15H05764]; and by the Strategic Promotion of Innovative Research and Development program of the Japan Science and Technology Agency [grant number 200904001].

References

[1] H.J. Hathaway, K.S. Butler, N.L. Adolphi, D.M. Lovato, R. Belfon, D. Fegan, T.C. Monson, J.E. Trujillo, T.E. Tessier, H.C. Bryant, D.L. Huber, R.S. Larson, E.R. Flynn, Detection of breast cancer cells using targeted magnetic nanoparticles and ultra-sensitive magnetic field sensors, Breast Cancer Res. 13 (2011) R108.
[2] N.B. Othman, T. Tsubaki, T. Yoshida, K. Enpuku, A. Kandori, Magnetic nanoparticle imaging using harmonic signals, IEEE Trans. Magn. 48 (2012) 3776–3779.
[3] J.J. Chieh, H.E. Horng, W.K. Tseng, S.Y. Yang, C.Y. Hong, H.C. Yang, C.C. Wu, Imaging the distribution of magnetic nanoparticles on Animal Bodies Using scanning SQUID biosusceptometry attached with a video camera, IEEE Trans. Appl. Supercond. 23 (2013) 1601503.
[4] D. Baumgarten, F. Braune, E. Supriyanto, J. Haueisen, Plane-wise sensitivity based

inhomogeneous excitation fields for magnetorelaxometry imaging of magnetic nanoparticles, J. Magn. Magn. Mater. 380 (2015) 255–260.
[5] B.W. Ficko, P. Giacometti, S.G. Diamond, Nonlinear susceptibility magnitude imaging of magnetic nanoparticles, J. Magn. Magn. Mater. 378 (2015) 267–277.
[6] B. Gleich, J. Weizenecker, Tomographic imaging using the nonlinear response of magnetic particles, Nature 435 (2005) 1214–1217.
[7] J. Rahmer, J. Weizenecker, B. Gleich, J. Borgert, Analysis of a 3-D system function measured for magnetic particle imaging, IEEE Trans. Med. Imaging 31 (2012) 1289–1299.
[8] E.U. Saritas, P.W. Goodwill, L.R. Croft, J.J. Konklw, K. Lu, B. Zheng, S.M. Conolly, Magnetic particle imaging (MPI) for NMR and MRI researchers, J. Magn. Reson. 229 (2013) 116–126.
[9] P. Vogel, M.A. Rückert, P. Klauer, W.H. Kullmann, P.M. Jakob, V.C. Behr, Traveling wave magnetic particle imaging, IEEE Trans. Med. Imaging 33 (2014) 400–407.
[10] C. Kaethner, M. Ahlborg, T. Knopp, T.F. Sattel, T.M. Buzug, Efficient gradient field generation providing a multi-dimensional arbitrary shifted field-free point for magnetic particle imaging, J. Appl. Phys. 115 (2014) 044910.
[11] S. Bai, A. Hirokawa, K. Tanabe, T. Sasayama, T. Yoshida, K. Enpuku, Narrowband magnetic particle imaging utilizing electric scanning of field free point, IEEE Trans. Magn. 51 (2015) 5101404.
[12] K. Enpuku, T. Miyazaki, M. Morishita, Y. Tsujita, M. Matsuo, S. Bai, T. Sasayama, T. Yoshida, Narrowband magnetic nanoparticle imaging using cooled pickup coil and gradient field, Jpn. J. Appl. Phys. 54 (2015) 057002.
[13] K. Enpuku, S. Bai, A. Hirokawa, K. Tanabe, T. Sasayama, T. Yoshida, The effect of Neel relaxation on the properties of the third harmonic signal of magnetic nanoparticles for use in narrow-band magnetic nanoparticle imaging, Jpn. J. Appl. Phys. 53 (2014) 103002.
[14] T. Morishige, T. Mihaya, S. Bai, T. Miyazaki, T. Yoshida, M. Matsuo, K. Enpuku, Highly sensitive magnetic nanoparticle imaging using cooled-Cu/HTS-superconductor pickup coils, IEEE Trans. Appl. Supercond. 24 (2014) 1800105.
[15] T. Knopp, T.F. Sattel, S. Biederer, J. Rahmer, J. Weizenecker, B. Gleich, J. Borgert, T.M. Buzug, Model-based reconstruction for magnetic particle imaging, IEEE Trans. Med. Imaging 29 (2010) 12–18.
[16] K. Sekihara, S.S. Nagarajan, Adaptive Spatial Filters for Electromagnetic Brain Imaging, Springer-Verlag, New York, USA, 2008.
[17] T. Yoshida, N.B. Othman, K. Enpuku, Characterization of magnetically fractionated magnetic nanoparticles for magnetic particle imaging, J. Appl. Phys. 114 (2013) 173908.